

RSC Advances



This is an *Accepted Manuscript*, which has been through the Royal Society of Chemistry peer review process and has been accepted for publication.

Accepted Manuscripts are published online shortly after acceptance, before technical editing, formatting and proof reading. Using this free service, authors can make their results available to the community, in citable form, before we publish the edited article. This *Accepted Manuscript* will be replaced by the edited, formatted and paginated article as soon as this is available.

You can find more information about *Accepted Manuscripts* in the [Information for Authors](#).

Please note that technical editing may introduce minor changes to the text and/or graphics, which may alter content. The journal's standard [Terms & Conditions](#) and the [Ethical guidelines](#) still apply. In no event shall the Royal Society of Chemistry be held responsible for any errors or omissions in this *Accepted Manuscript* or any consequences arising from the use of any information it contains.

Clathrate directed assembly of tetrapyridyl-tetra phenylethylene metal organic frameworks

Sam L. Jackson, Anushri Ranaware, Colin Rix, Sheshanath V. Bhosale*, and Kay Latham*

Received 00th January 20xx,
Accepted 00th January 20xx

DOI: 10.1039/x0xx00000x

www.rsc.org/

This work focuses on three 2-D MOFs based on the ligand tetrapyridyltetraphenylethylene (tppe) with the metal ions: manganese(II), nickel(II) and copper(II). These all networks are highly microporous with rhomboid channels measuring $\sim 14 \times 17 \text{ \AA}$ giving approximately 49% solvent accessible void space. These voids are filled with ordered tetrachloroethylene (TCE) molecules that act as structure directing agents, and the structures remain porous even after removal of TEC Molecules. The networks were characterised *via* single crystal X-ray diffraction, powder XRD, TGA, FTIR, fluorescence spectroscopy, and elemental analysis. Gas absorption measurements on the desolvated networks indicate that the networks are moderately selective, and their behaviour was typical of similar MOF networks. The Ni^{2+} based tppe-MOF exhibited greater capacity to absorb polar gases despite structural similarities to the other networks.

Introduction

Metal organic frameworks (MOFs) are a significant class of porous, tuneable crystalline networks which consist of metal ions or clusters connected by organic ligands. They have generated tremendous interest due to their low density, ultra-high porosity and topologically diverse structures, with applications in gas storage¹⁻⁹, catalysis¹⁰⁻¹⁵, sensing¹⁶⁻¹⁸ and various other functions¹⁹. A vast number of networks with a large range of pore sizes and adjustable properties have been synthesised. The fundamental challenge in MOF synthesis is designing a target structure that has predictable behaviour for its intended application. Several attempts have been made to systematise this process⁶, but no universally successful approach has emerged to predict these structures. A further synthetic complication is the possible role of solvent as a template agent akin to the role of dissolved Me_4N^+ ions, for example, in tailoring zeolite sites during hydrothermal synthesis.²⁰

Tetraphenylethylene (TPE) is the parent of a family of compounds comprised of four phenyl rings around a central ethylene bond. The rings are orientated in a characteristic 'propeller' conformation around the central bond, where each phenyl ring is staggered relative to the opposite ring. This orientation persists for its derivatives and prevents reduction of the ethylene. The extended π -conjugation gives TPE derivatives which possess exploitable optical properties²¹. They are non-emissive in solution, as rotation of the phenyl rings and twisting of the C=C bond in the excited state allows for non-radiative relaxation, however when aggregated in

solution, and in the solid state, these processes no longer exist. Therefore aggregation-induced enhanced fluorescent emission (AIEE) occurs in almost all TPE derivatives.²² In recent years, tetrapyridyl-substituted TPE (tppe) derivatives have been reported for various applications such as supramolecular building blocks²³, organic and metal-organic networks²⁴⁻²⁶, mercury sensing²⁶ and halogen bonded networks²⁷. The tppe molecule (Fig. 1) is of particular interest due to its ability to act as a ligand, its size, rigidity and propensity to undergo aggregation-induced enhanced emission (AIEE)²⁸. Networks utilizing carboxylic substituted tppe have demonstrated tuning of the fluorescence of tppe²⁹, highly thermally stable NH_3 sensors³⁰ and the sensing of volatile organic compounds³¹. Recently, several crystal engineered structures of tppe-based derivatives have been described, such as those of the Wang *et al.* group,²⁵ who reported a discrete 3D tetragonal prism of TPE, dipyrindine and a platinum metal. In another report, Icli's group³² described a similar phenomenon utilizing borole benzenes with various pyridyl ligands. Recently, Gong *et al.*³³ reported a novel Zn(II) organic framework of tppe with the co-ligand btc(benzene-1,3,5-tricarboxylic acid).

Herein, we report the synthesis of three novel porous metal organic frameworks (PMOF), using tppe as an organic building block and Mn^{2+} , Ni^{2+} and Cu^{2+} as metal linkers. The structures of the PMOFs were characterized by their single-crystal X-ray structures, PXRD, fluorescence and FTIR spectroscopy. The thermal and gas absorption properties reported exhibit predicted structural hysteresis properties.

School of Applied Sciences, RMIT University, GPO Box 2476, Melbourne, VIC-3001, Australia

* sheshanath.bhosale@rmit.edu.au; kay.latham@rmit.edu.au

Electronic Supplementary Information (ESI) available: [Details of TGA, FTIR, SC-XRD, powder XRD, TGA-GC available in ESI]. See DOI: 10.1039/x0xx00000x

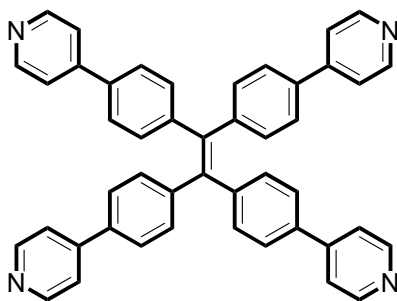


Fig. 1 Tetrapyrrolyl-tetraphenylethylene (tpe) derivative used for this study.

Experimental

General details

MnCl₂•4H₂O, NiCl₂•6H₂O, CuCl₂•2H₂O, tetrabromo-TPE, Pd(PPh₃)₄, 4-pyridine boronic acid, 2,3-dimethyl-2-butene, methanol (MeOH) tetrachloroethylene (TCE) and CHCl₃ were all used as received from Sigma-Aldrich, unless otherwise stated. FTIR spectra were collected on a Perkin-Elmer Spectrum 100 FTIR spectrometer at room temperature in the range 650-4000 cm⁻¹ using an ATR attachment. Nitrogen absorption-desorption measurements were carried out on a Micromeritics ASAP2000 at 77K. Prior to the tests, the samples were degassed at 150 °C in order to remove the tetrachloroethylene trapped in the pores. Specific surface areas were determined using the Brunauer-Emmett-Teller (BET) equation over the range of relative pressures between 0.01 and 0.3p/p°. The pore size distribution was calculated by applying the non-local density functional theory (NLDFT) method. TGA analysis was performed under nitrogen gas (20 °C min⁻¹) using a Pyrex-7. PXRD patterns were collected under ambient conditions on a Bruker D4 ENDEAVOR diffractometer, fitted with a Lynx-Eye position sensitive detector, using CuKα radiation (λ = 1.5406Å). Calculation of the structural and electronic properties of [(MnCl₂)tpe] was carried out using the pseudopotential density functional theory (DFT) code CASTEP³⁴ (v6.1) within the local density approximation exchange correlation functional. Calculations were performed using plane waves with a 300 eV kinetic energy cut-off and on-the-fly generated pseudopotentials. A single gamma centred k point was using to sample the brillouin zone. A Pulay density mixing scheme was used in the self-consistent field calculations with a minimum total energy/ atom convergence tolerance of 1×10⁻⁵ eV. The program Jmol³⁵ was used for visualization.

Fluorescence measurements were performed on a Horiba FluoroMax Plus using a solid-state holder. Samples were excited using a 150W Xenon arc lamp at 400nm and then the emission measured from 415nm to 650nm.

Synthesis of tetrapyrrolyl-tetraphenylethylene (tpe)

The ligand tpe was prepared *via* a Suzuki coupling reaction of tetrabromo-TPE with 4-pyridine boronic acid in the presence of Pd(PPh₃)₄, following a literature procedure (Fig 1).^{28,36}

Preparation of [(MnCl₂)tpe]•3.5TCE

[(MnCl₂)tpe]•3.5TCE was prepared by dissolving 95mg (0.48mmol) of MnCl₂•4H₂O in 40mL methanol and then gently layering this over a solution of 75mg (0.12 mmol) of tpe in 60mL 3:1 TCE:MeOH. After 3 days, small yellow crystals formed on the walls of the vessel. These were separated from the solution by centrifugation at 30,000RPM for 10 minutes, air dried and obtained in 46.1% yield. Elemental analysis: calcd for [(MnCl₂)tpe]•3.5TCE C,46.28; N,3.92; H,2.26%. Found: C, 46.62; N,3.85; H,2.28%. The elemental analysis suggests that the compound undergoes a partial loss of TCE molecules at room temperature.

Preparation of [(NiCl₂)tpe]•3TCE

[(NiCl₂)tpe]•3TCE was prepared by dissolving 100mg (0.48mmol) of NiCl₂•6H₂O in 40mL methanol and then gently layering this over a solution of 100mg (0.16mmol) of tpe in 60mL of 3:1 TCE:MeOH. After 3 days, small green crystals formed at the solvent interface. These were separated from the solution by centrifugation at 30,000 RPM for 10 minutes, air dried and obtained in 66.6% yield. Elemental analysis: calcd for [(NiCl₂)tpe]•3TCE C,49.26; N,4.15; H,2.54%. Found C,49.21; N,4.06; H,2.49%.

Preparation of [(CuCl₂)tpe]•3.5TCE

[(CuCl₂)tpe]•3TCE was prepared by dissolving 108.8mg (0.48mmol) of CuCl₂•2H₂O in 40mL methanol and then gently layering this over a solution of 100mg (0.16mmol) of tpe in 60mL of 3:1 TCE:MeOH. After 3 days, small green crystals formed at the solvent interface. Elemental analysis was not performed due to the instability of the Cu²⁺ network when separated from solution.

Preparation of [(MnCl₂)tpe]•3.5(2,3-dimethyl-2-butene)

[(MnCl₂)tpe]•3.5(2,3-dimethyl-2-butene) was prepared by dissolving 108.8mg (0.48mmol) of MnCl₂•6H₂O in 40mL methanol and then gently layering this over a solution of 100mg (0.16mmol) of tpe in 60mL of 3:1 2,3-Dimethyl-2-butene:MeOH. After 14 days, small colourless crystals formed on the walls of the vessel. These were separated from the solution by centrifugation at 30,000 RPM for 10 minutes, air dried and obtained in 26.7% yield.

Preparation of networks in the absence of TCE

Similar layered systems were prepared using CHCl₃, MeOH and THF in place of TCE. None of these systems produced any solid product.

Crystallography

Single crystal X-ray diffraction intensities were collected on a Bruker APEX II diffractometer with a PHOTON 100 CCD and Mo-Kα radiation (λ = 0.71073Å) at 200K. The data were corrected for Lorentz and polarization effects. Absorption corrections were carried out based on multiple-scanned reflections. The crystal structures were solved by direct methods using SHELX-2014/7 and refined by full-matrix least

square refinement on F^2 using SHELX-2014/7. All non-hydrogen atoms were refined with anisotropic displacement parameters. The refinement of the solvent molecules in $[(\text{CuCl}_2)\text{tppe}]\cdot 4\text{TCE}$ required some distance and similarity restraints. The $[(\text{MnCl}_2)\text{tppe}]\cdot 4(2,3\text{-dimethyl-2-butene})$ structure exhibited some disorder in both rings in the central TPE and the outer pyridine rings. Distance and position restraints were required for both these and for the solvent molecules. The hydrogen atoms were all placed at geometrically calculated positions and refined with a site occupancy factor of 0.5 while allowing them to ride on the parent atom. Crystal and refinement details are given in Table 1 for the Cu(II) and Mn(II) derivatives. The largest difference peaks were $0.87\text{e}\text{\AA}^{-3}$ in the structure of $[(\text{CuCl}_2)\text{tppe}]\cdot 4\text{TCE}$, $0.88\text{e}\text{\AA}^{-3}$ for $[(\text{MnCl}_2)\text{tppe}]\cdot 4\text{TCE}$ and $0.34\text{e}\text{\AA}^{-3}$ for $[(\text{MnCl}_2)\text{tppe}]\cdot 4(2,3\text{-dimethyl-2-butene})$.

Gas absorption

A crystalline sample of $[(\text{MnCl}_2)\text{tppe}]\cdot 4\text{TCE}$ was transferred to a sample cell and heated overnight at a temperature of $250\text{ }^\circ\text{C}$ under dynamic vacuum. The activated sample, of weight 85mg, underwent CO_2 , H_2 and CH_4 isothermal absorption/desorption measurements. During the measurements the sample was heated at a temperature of $250\text{ }^\circ\text{C}$ under dynamic vacuum for a period of two hours. High pressure CO_2 , H_2 and CH_4 volumetric gas sorption data were measured using a Sieverts-type BELsorp-HP automatic gas sorption apparatus (BEL Japan Inc.). Ultra-high purity CO_2 , H_2 , CH_4 and He (helium was used as an inert gas) used for sorption studies were purchased from BOC or Air Liquide. Non-ideal gas behaviour at high pressures of each gas at each measurement and reference temperature was corrected. Source data were obtained from the NIST fluid properties website.³⁷ Sample compartment temperatures ranging from 258–298K were controlled by a Julabo F25-ME chiller/heater that re-circulated fluid at $\pm 0.1\text{ }^\circ\text{C}$ through a capped, jacketed stainless steel flask housed within a polystyrene box. A calibrated external Pt 100 temperature probe monitored the flask temperature. Cryogenic temperatures were maintained with a BEL liquid N_2 level controller. Samples were kept at the measurement temperature for a minimum of 1 hr after the desired temperature had been achieved to allow full thermal equilibrium to be attained before data measurement commenced. The isosteric heats of CO_2 and CH_4 sorption were calculated using a least-squares fitting of a virial -type thermal absorption equation that modeled $\ln(P)$ as a function of the amount of surface excess of gas sorbed over the measurement temperatures 258K and 273K³⁸. Optimized virial coefficients and R^2 values are given (see ESI Table S1-2). Data was collected in a similar manner for $[(\text{NiCl}_2)\text{tppe}]\cdot 4\text{TCE}$.

Results and discussion

Crystals of the manganese complex $[(\text{MnCl}_2)\text{tppe}]\cdot 4\text{TCE}$ adopt an orthorhombic structure (Acaa) with octahedrally-coordinated metal centres (Table 1). Each manganese ion is coordinated to four pyridine rings in the equatorial positions

and two chloride ions in the axial positions. The asymmetric unit contains three crystallographically-independent MnCl_2 , four TCE molecules and one tppe moiety. The structure consists of polymeric 2D flat layers with rhomboidal pores. The topology of the 2D network is a square grid of (4,4) type as shown in Fig. 2 and ESI Fig. S1.

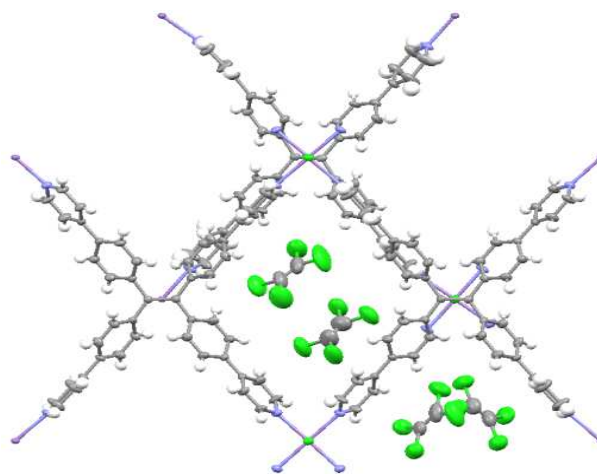


Fig. 2 3D structure of $[(\text{MnCl}_2)\text{tppe}]\cdot 4\text{TCE}$ along a axis

The Mn^{2+} ion and the central tppe ethylene bond reside on a crystallographic centre of inversion around a twofold axis. The crystallographic position of the Mn^{2+} ions requires that each alternate ion coordinates with pairs of pyridyl rings that are either co-planar or in a 'propeller' coordination (Fig. 3). The Mn-N and Mn-Cl distances are in the range of 2.31–2.36Å and 2.45–2.48Å respectively. The N-Mn-N angles are in the range 91.83–93.89° and 86.11–88.18°, and the Cl-Mn-Cl angles are 180°. These are typical bond lengths and angles for an octahedral manganese complex (see ESI Fig. S2-4 and Table S5-6). The channels are rhomboidal in section, as a result of the orientation of the ligand, and propagate through the network. They are either $14.716 \times 17.211\text{\AA}$ or $13.339 \times 17.211\text{\AA}$ depending on the orientation of the central tppe ethylene bond relative to the pore TCE guest molecules occupy the rhomboid pores within the sheets.

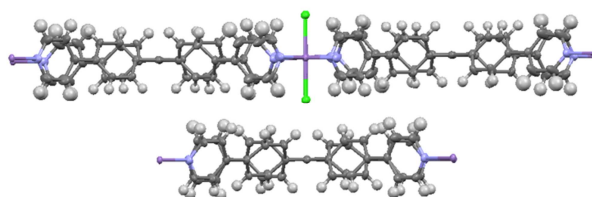


Fig. 3 Structure of $[(\text{MnCl}_2)\text{tppe}]\cdot 4\text{TCE}$ along the b axis.

The 2D layers in the structure are offset along the a axis (Fig 3.) with an interlayer distance of 3.40\AA . The chlorides are placed directly over the ethene bonds in the adjacent layers. The rings are adjacent to their counterparts in the other layers but show no significant π - π interaction. The TCE molecules are positioned between the 2D planes. The alternating nature of the pores organises the TCE into a regular

motif of two TCE molecules contained within the confining phenyl rings. Therefore, there are four TCE molecules for every tppe molecule. They form a chain of alternating molecules with each pair of two TCE molecules perpendicular to the following two. The crystallographic centre of inversion lies between the pair of TCE molecules. This is noteworthy as it resembles the work of Seidel,³⁹ using a similar layered system with porphyrin as the ligand and TCE as the solvent. However, neither of the two porphyrin systems exhibit the alternating motif (Fig. 4) observed in the $[(\text{MnCl}_2)\text{tppe}]\cdot 4\text{TCE}$ structure, as both have layers intercalated by solvent molecules.

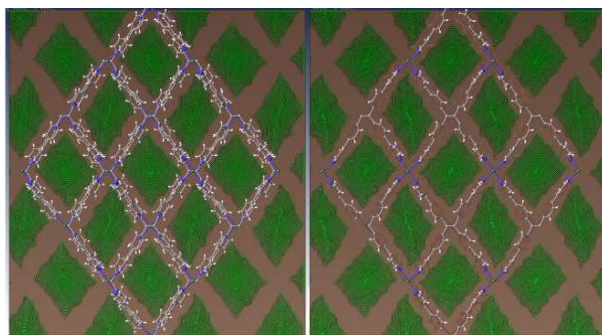


Fig. 4 Void space visualization of $[(\text{MnCl}_2)\text{tppe}]$

The network junctions resemble classical Werner clathrates in that they have the general formula $\text{M}(\text{py})_4\text{X}_2$, where X is a halide and M is a divalent metal ion. Werner clathrates are known to be highly stereoselective for intercalated molecules and this has been observed in our networks. Previous attempts to synthesize similar PMOFs based on Mn^{2+} and Ni^{2+} , using DMF as a solvent in a solvothermal method, have failed. However, some success has been reported for the formation of these PMOFs with zinc(II).¹⁰ Our own attempts in polar solvents such as MeOH and in non-polar chlorinated solvents were unsuccessful. Only by using a similarly structured non-chlorinated 2,3-dimethyl-2-butene (DMB) as a replacement solvent, was the synthesis successful. When used in place of TCE, it performs a similar role. Indeed the butene adopts an identical orientation in the pores to TCE. (See ESI Fig. S9-10) The crystal structure remains essentially unchanged with some alterations to symmetry elements. The network also exhibits more disorder around both the central tppe moiety and the outer pyridine rings. Therefore the stereochemical positioning of TCE and DMB in the voids, and their relationship with the tppe, are key to understanding the crystallization of these networks.

In order to better understand the nature of the interaction between the TCE molecules and the network molecules, calculation of the electronic properties of $[(\text{MnCl}_2)\text{tppe}]$ was carried out using the pseudopotential density functional theory (DFT) code CASTEP³⁴, with the structural data used as the model to investigate the interaction between the solvent and the MOF skeletal framework. The pseudopotential electron density calculations confirm the alternating structural nature of the pores as the cause of the TCE molecule orientation. As seen in Fig. 5, there is a uniform electron

density over the framework with a very low electron population in the voids. The calculations also confirm the alternating nature of the pores (Fig. 5).

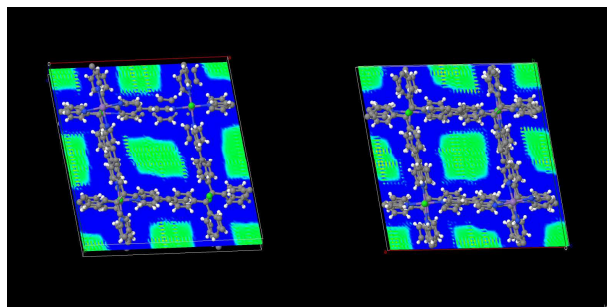


Fig. 5 Pseudopotential density visualization of $[(\text{MnCl}_2)\text{tppe}]$

density over the framework with a very low electron population in the voids. The calculations also confirm the alternating nature of the pores (Fig. 5). Altering the metal ion causes the network to undergo subtle changes as evidenced from the SCXRD. The $[(\text{CuCl}_2)\text{tppe}]\cdot 4\text{TCE}$ structure is isomorphous to that of the Mn^{2+} analogue with small differences in the bond distances (2.32-2.51 Å, 2.44-2.48 Å) and angles (92.11-94.01° and 85.99-87.90°), which show no evidence of any significant Jahn-Teller structural distortion. The pores have a similar alternating structure with TCE in identical positions as would be expected if TCE was acting as a structure directing agent. (See ESI Fig. S6-8 and Table S11-12). The network is unstable upon exposure to air and changes from a crystalline blue solid to an amorphous green powder. FTIR Analysis of the amorphous solid (See ESI Fig S11) confirms the presence of water, which is also supported by TGA analysis. We hypothesise that the structure absorbs water from the air, which displaces the tppe ligand and the network subsequently collapses. It is noted that Tan et al.⁴⁰ observed similar behaviour with the displacement of DABCO by water molecules in a related system.

An isostructural Ni²⁺ network has also been synthesised which was characterised by FTIR, PXRD and GC-MS/TGA. Unfortunately, SCXRD analysis was unsuccessful. However, there is considerable evidence to suggest that the network is similar to that of the Cu²⁺ and Mn²⁺ structures. For example, the PXRD pattern of the Ni²⁺ network (Fig. 7a) is a close match to that of the experimental PXRD data of the Mn²⁺ network, and the simulated PXRD data created from the SCXRD data of the Cu²⁺ network. This is also supported by similarities in the FTIR data of the three networks (see ESI Fig. 12-14). The FTIR spectra of each of the three networks have a strong sharp peak around at 910cm⁻¹ and a series of sharp peaks at 802cm⁻¹, 776cm⁻¹, 757cm⁻¹, which indicate the presence of C-Cl bonds. The presence of the ligand was also confirmed via FTIR(see ESI Fig.15).

Fluorescence spectra

Both [(MnCl₂)tpe]•4TCE and [(NiCl₂)tpe]•4TCE are markedly fluorescent in the solid state, and their spectra are significantly different to the spectra of pure tpe ligand (Fig. 6). The spectrum of the manganese network is more intense and

centred around the ligand wavelength without an increase in intensity or a shift in wavelength. The lack of an increase in intensity may be attributed to an alternative relaxation pathway.

Fluorescence spectra of the evacuated networks were also collected (See ESI Fig. 16-17). Removal of the TCE had no significant effect on the fluorescence. Given what has been hypothesized about the pathways for the fluorescence of the network, this is to be expected.

Table 1. Details of crystal data and structure refinement parameters of [(MnCl₂)tpe]•4TCE and [(CuCl₂)tpe]•4TCE

	[(MnCl ₂)tpe]•4TCE (ccdc:1412453)	[(CuCl ₂)tpe]•4TCE (ccdc:1412223)	[(MnCl ₂)tpe]•4DMB(ccdc: 1423185)
Empirical formula	C ₄₆ H ₃₂ Cl ₂ Mn N ₄ , 4(C ₂ Cl ₄)	C ₄₆ H ₃₂ Cl ₂ Cu N ₄ , 4(C ₂ Cl ₄)	C ₄₆ H ₃₂ Cl ₂ Mn N ₄ , 4(C ₆ H ₁₂)
Mr	1429	1438	996.81
Crystal size	0.555 × 0.075 × 0.058	0.115 × 0.104 × 0.047	0.417x0.358x0.326
Crystal color	Clear yellow	Clear blue	Clear colourless
Crystal system	Orthorhombic	Orthorhombic	monoclinic
Space group	A c a a	A c a a	P2/n
T[K]	200(1)	200(1)	200(1)
a[Å]	23.717(4)	23.675(3)	14.5708(13)
b[Å]	29.432(5)	29.299(4)	12.2088(12)
c[Å]	34.422(6)	34.539(4)	17.3624(17)
α[o]	90	90	90
β[o]	90	90	90.061(2)
γ[o]	90	90	90
Z	16	16	2
Dcalc	1.581	1.595	1.072
μ[mm ⁻¹]	1.062	1.209	0.338
2θmax[o]	25.002	24.300	29.998
Data collected	229353	70692	29104
Refined	698/34	698/34	524/313
Goodness of Fit on	1.031	1.016	1.098
R1[I>2σ(I)]	0.0875	0.0857	0.0522
wR2(all data)	0.2856	0.3088	0.1908

centred around 523nm. This enhanced emission is significantly red-shifted compared to the corresponding band for the ligand (463 nm). We attribute this shift to the network reducing non-radiative decay pathways by hindering vibrational and rotational relaxation processes. This is also believed to contribute to the increased emission. In contrast, the [(NiCl₂)tpe]•4TCE exhibits a series of fine structure peaks

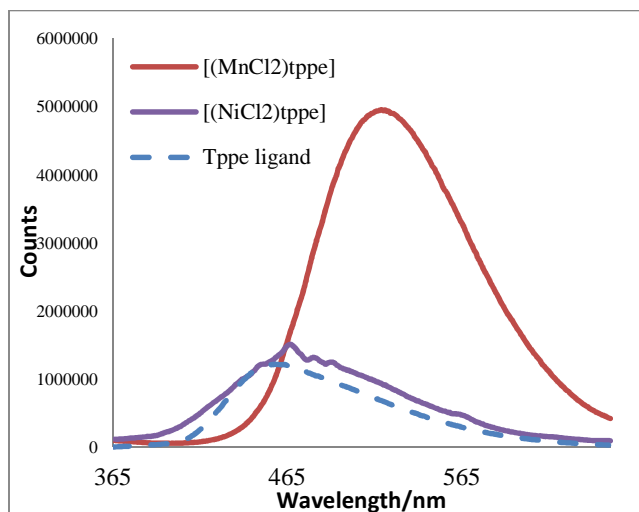


Fig. 6 Fluorescence comparison of $[(\text{MnCl}_2)\text{tppe}]$, $[(\text{NiCl}_2)\text{tppe}]$, and tppe ligand.

Thermogravimetric analysis

The thermal decomposition behaviour of $[(\text{MnCl}_2)\text{tppe}] \cdot 4\text{TCE}$ in N_2 was studied in the range 50–750°C (see ESI Fig. S18). Thermogravimetric analysis indicated a weight loss of 35% over the temperature range 75–200°C, which correlated with the loss of 3.5 mol TCE per 1 mol tppe. The gaseous exhaust generated by this weight loss was analysed via FTIR (see ESI fig. S19) and was found to contain strong, sharp peaks at 910cm^{-1}

and 767cm^{-1} , and a broad weak peak at 2350cm^{-1} . The sharp peaks at the lower frequency correspond to the expected range for a C–Cl stretching. This is confirmed by comparison with literature spectra. The broader 2350cm^{-1} peak was seen throughout the analysis and corresponds with the anti-symmetrical stretch of carbon dioxide. This is expected as carbon dioxide impurities are known to be present in the carrier gas. Once the sample had lost 10% of its weight, GC-MS was performed on the exhaust. The resultant spectra had peaks at 166, 131, 94 m/z corresponding both the calculated mass of TCE and its literature spectrum (see ESI Fig. 20).

There is a second weight loss at 425–475°C, which can be attributed to the loss of the remaining 0.5 mol TCE and pyrolysis of the ligand. Above 750°C air was introduced, leading to an immediate combustion, leaving only a small amount (9%) of metal oxide residue. By measuring the variation in the intensity of a single infrared frequency over the course of the thermal analysis (see ESI fig. S21), we endeavoured to identify the departing species. Tetrachloroethene (910cm^{-1}) dominated the initial weight loss and was also present in the second weight loss. In addition carbon dioxide, although absolute measurements were unreliable, was generated during the second weight loss. These measurements indicate that the TCE can be removed without distortion of the structure at temperatures lower than 450°C, and this is confirmed by PXRD (Fig. 6a). Identical measurements were performed on the Ni^{2+} network, which

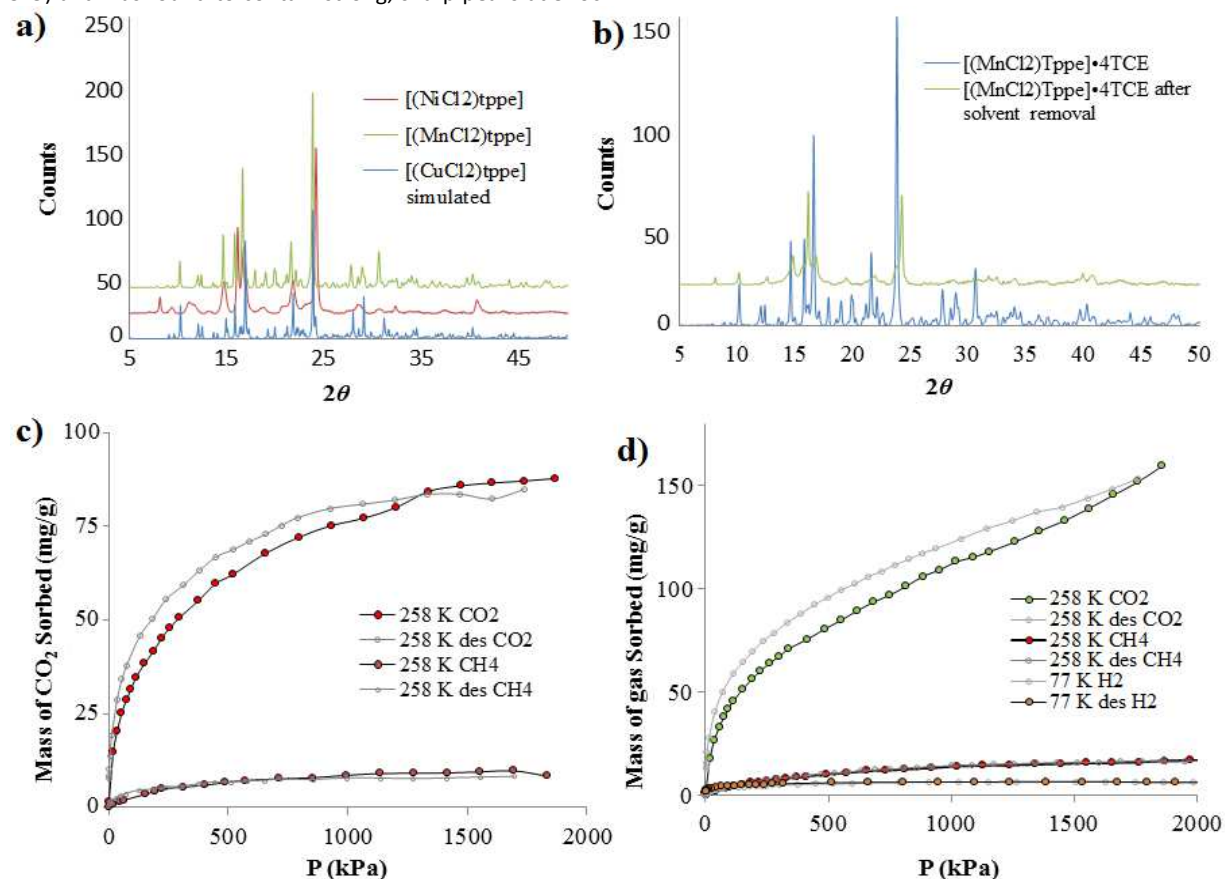


Fig. 7 a) PXRD of $[(\text{MnCl}_2)\text{tppe}] \cdot 4\text{TCE}$, $[(\text{NiCl}_2)\text{tppe}] \cdot 4\text{TCE}$ and simulated $[(\text{CuCl}_2)\text{tppe}] \cdot 4\text{TCE}$ b) PXRD of $[(\text{MnCl}_2)\text{tppe}] \cdot 4\text{TCE}$ before and after solvent removal c) Gas absorption isotherm for CO_2 and CH_4 on $[(\text{MnCl}_2)\text{tppe}]$. d) Gas absorption isotherm for CO_2 and CH_4 on $[(\text{NiCl}_2)\text{tppe}]$.

10xx

exhibited similar behaviour with a weight loss of 40% over 75–200 °C and a second weight loss at 425–475 °C. It also demonstrated complete combustion of the ligand when exposed to oxygen at 750 °C with 6.5% metal oxide residue remaining. The thermal behaviour of $[(\text{CuCl}_2)\text{tpe}] \cdot 4\text{TCE}$ proved difficult to obtain as the network rapidly decayed when exposed to air, which also frustrated attempts to directly determine a PXRD. Therefore, a simulated version was obtained using the software program, Mercury (see ESI Fig. S24). Thus, the $[(\text{MnCl}_2)\text{tpe}] \cdot 4\text{TCE}$ and $[(\text{NiCl}_2)\text{tpe}] \cdot 4\text{TCE}$ networks are believed to be stable after solvent removal, as they do not undergo any weight loss or structural changes between 200–400 °C. This is noteworthy, since it is an extremely high thermal stability for a pyridine network. Given the porosity of the networks upon removal of the solvent, it is likely other molecules could be inserted into the voids that are present in the network. Appropriate candidates for this are the gases: CO_2 , CH_4 and H_2 .

Gas absorption

Prior to the gas absorption studies on the $[(\text{MnCl}_2)\text{tpe}]$, the solid samples were heated at 250 °C in vacuum to remove the TCE solvent. The PXRD patterns observed before and after solvent removal are presented in Fig. 7b, and suggest that the overall network structure remains essentially unchanged upon removal of the clathrated TCE from the voids. The CO_2 and CH_4 isotherms are depicted in Fig. 7c. The data for CO_2 absorption corresponds to a type-I isotherm characteristic of a microporous material. The BET and Langmuir areas are $405.9 \text{ m}^2/\text{g}$ and $501.4 \text{ m}^2/\text{g}$ respectively.

The CO_2 absorption isotherm for $[(\text{MnCl}_2)\text{tpe}]$ at 258K demonstrates a maximum uptake of 8.07wt%, which is comparable to existing networks⁴¹. The CO_2 isotherm does not exhibit a plateau at higher pressures suggesting a cooperative absorptive process.

The CH_4 absorption isotherm exhibited a maximum uptake of only 0.88wt%; the enthalpy of absorption is 27.2kJ/mmol for CO_2 and 13.1kJ/mmol for CH_4 . The significantly lower CH_4 absorption is typical of all reported networks to date. In addition, the network does not appear to uptake either N_2 or H_2 gas suggesting that it can only absorb polar gases.

The CO_2 absorption isotherm for $[(\text{NiCl}_2)\text{tpe}]$ at 258K (Fig. 7d) demonstrates a maximum uptake of 13.7wt%, a considerable improvement over the Mn^{2+} network.

The CH_4 absorption isotherm exhibited a maximum uptake of only 1.11wt%; the enthalpy of absorption is 27.2kJ/mmol for CO_2 and 19.4kJ/mmol for CH_4 . The H_2 absorption isotherm indicates fully reversible uptake of 0.63wt % at 1kPa. In contrast, to the Mn^{2+} network, the Ni^{2+} network absorbs both N_2 and H_2 , although only weakly. It also exhibits stronger absorption of both CH_4 and CO_2 compared to the Mn^{2+} network (see ESI Fig. S25–30). Similar measurements on the Cu^{2+} network were precluded by its instability in air.

Conclusions

Three metal organic frameworks $[(\text{MnCl}_2)\text{tpe}] \cdot 4\text{TCE}$, $[(\text{NiCl}_2)\text{tpe}] \cdot 4\text{TCE}$ and $[(\text{CuCl}_2)\text{tpe}] \cdot 4\text{TCE}$ have been synthesised and the structures of the Mn^{2+} and Cu^{2+} networks determined *via* X-ray crystallography. The syntheses were only possible in the presence of TCE and 2,3-dimethyl butene, suggesting that the molecular topography about the ethylene bond is acting as a structure directing agent during the synthesis. This demonstrates the crucial, but unpredictable role, that foreign molecules can perform during molecular self-assembly in solution. The copper network collapses upon removal from solvent. This appears to be due to hydrolysis. The structures resemble Werner clathrates. The work reported here highlights the potential of TPE to act as an easily-synthesised ligand based on a rigid ethylene platform. The networks also continue to display the fluorescent properties of tpe modulated according to the coordinating metal. The resultant PMOF networks were shown to be stable upon removal of the clathrated solvent up to 450 °C, and to retain their porosity upon solvent removal. Gas absorption measurements on the desolvated networks indicate that the networks are moderately selective, and their behaviour was typical of similar MOF networks. The $[(\text{NiCl}_2)\text{tpe}]$ exhibited greater capacity to absorb polar gases despite structural similarities to the other networks.

Acknowledgements

S.J. acknowledges RMIT PhD Scholarship 2014. S.V.B. Acknowledges Australian Research Council for financial support under a Future Fellowship Scheme (FT110100152). The authors acknowledge the Australian Microscopy & Microanalysis Research Facility at RMIT University, Dr Keith White (University of Melbourne) for gas absorption work, Nicholas L. McDougall for the CASTEP calculations and the Campbell Microanalytical Laboratory, New Zealand for elemental analysis.

Notes and references

Note: Elemental analysis network has been exposed to air and has excluded some of TCE molecule over time, thus showing 3.5TCE molecules. However, in X-ray, TGA and PXRD analysis samples have been rapidly dried thus showing 4TCE molecules.

1. R. E. Morris and P. S. Wheatley, *Angewandte Chemie*, 2008, **47**, 4966–4981.
2. X. Lin, J. Jia, X. Zhao, K. M. Thomas, A. J. Blake, G. S. Walker, N. R. Champness, P. Hubberstey and M. Schroder, *Angewandte Chemie*, 2006, **45**, 7358–7364.
3. T. A. Makal, J. R. Li, W. Lu and H. C. Zhou, *Chemical Society reviews*, 2012, **41**, 7761–7779.
4. J. Graetz, *Chemical Society reviews*, 2009, **38**, 73–82.
5. S. L. Chaoying Gao, * Linhua Xie, Chunyan Sun, Jianfang Cao, Yuanhang Ren, Dan Feng and a. Z. Su, *Yearbook of Pathology and Laboratory Medicine*, 2008, **2009**, 177–182.
6. J. Y. Lee, L. Pan, X. Huang, T. J. Emge and J. Li, *Advanced Functional Materials*, 2011, **21**, 993–998.

7. J.-F. V. Nour Nijem, Lingzhu Kong, Kunhao Li, Sanhita Pramanik, Yonggang Zhao, Jing Li, David Langreth, and Yves J. Chabal, *Journal of American Chemical Society*, 2009, **132**, 1654-1664.
8. D. Fairen-Jimenez, N. A. Seaton and T. Duren, *Langmuir : the ACS journal of surfaces and colloids*, 2010, **26**, 14694-14699.
9. I. T. Xiang Lin, Alexander J. Blake, Anne Dailly, Craig M. Brown,, M. Z. Jason M. Simmons, Gavin S. Walker, K. Mark Thomas, and P. H. Timothy J. Mays, Neil R. Champness, and Martin Schroder, *Journal of American Chemical Society*, 2008, **131**, 2159-2171.
10. M. Yoon, R. Srirambalaji and K. Kim, *Chemical reviews*, 2012, **112**, 1196-1231.
11. J. Lee, O. K. Farha, J. Roberts, K. A. Scheidt, S. T. Nguyen and J. T. Hupp, *Chemical Society reviews*, 2009, **38**, 1450-1459.
12. M. D. Satoshi Horike, Kentaro Tamaki and Jeffery R. Long, *Journal of American Chemical Society*, 2008, **130**, 5854-5855.
13. M. Savonnet, S. Aguado, U. Ravon, D. Bazer-Bachi, V. Lecocq, N. Bats, C. Pinel and D. Farrusseng, *Green Chemistry*, 2009, **11**, 1729.
14. J. M. Roberts, B. M. Fini, A. A. Sarjeant, O. K. Farha, J. T. Hupp and K. A. Scheidt, *Journal of the American Chemical Society*, 2012, **134**, 3334-3337.
15. D. Feng, Z. Y. Gu, J. R. Li, H. L. Jiang, Z. Wei and H. C. Zhou, *Angewandte Chemie*, 2012, **51**, 10307-10310.
16. B. Chen, L. Wang, Y. Xiao, F. R. Fronczek, M. Xue, Y. Cui and G. Qian, *Angewandte Chemie*, 2009, **48**, 500-503.
17. L. E. Kreno, K. Leong, O. K. Farha, M. Allendorf, R. P. Van Duyne and J. T. Hupp, *Chemical reviews*, 2012, **112**, 1105-1125.
18. Y. T. Hai-Long Jiang, Zhang-Hui Lu, and Qiang Xu, *Journal of American Chemical Society*, 2010, **132**, 5586-5587.
19. P. Horcajada, R. Gref, T. Baati, P. K. Allan, G. Maurin, P. Couvreur, G. Ferey, R. E. Morris and C. Serre, *Chemical reviews*, 2012, **112**, 1232-1268.
20. R. Chal, C. Gérardin, M. Bulut and S. van Donk, *ChemCatChem*, 2011, **3**, 67-81.
21. P. P. Kapadia, Doctor of Philosophy degree in Chemistry, The University of Iowa, 2011.
22. Z. L. X. J. D. Luo, J. W. Y. Lam, L. Cheng, H. Y. Chen, C. F. Qiu, H. S. Kwok, X. W. Zhan, Y. Q. Liu, D. B. Zhu and B. Z. Tang, *Chem. Commun.*, 2001, 1740.
23. P. P. Kapadia, J. C. Widen, M. A. Magnus, D. C. Swenson and F. C. Pigge, *Tetrahedron Letters*, 2011, **52**, 2519-2522.
24. B. Kilbas, S. Mirtschin, R. Scopelliti and K. Severin, *Chemical Science*, 2012, **3**, 701.
25. M. Wang, Y. R. Zheng, T. R. Cook and P. J. Stang, *Inorganic chemistry*, 2011, **50**, 6107-6113.
26. G. Z. a. D. Z. G. Huang, *Chem. Commun.*, 2012, **48**, 7504.
27. F. C. Pigge, P. P. Kapadia and D. C. Swenson, *CrystEngComm*, 2013, **15**, 4386.
28. S.-K. K. B.-K. An, S.-D. Jung and S. Y. Park, *J. Am. Chem. Soc.*, 2002, **124**, 14410.
29. Z. Wei, Z.-Y. Gu, R. K. Arvapally, Y.-P. Chen, R. N. McDougald, J. F. Ivy, A. A. Yakovenko, D. Feng, M. A. Omary and H.-C. Zhou, *Journal of the American Chemical Society*, 2014, **136**, 8269-8276.
30. N. B. Shustova, A. F. Cozzolino, S. Reineke, M. Baldo and M. Dincă, *Journal of the American Chemical Society*, 2013, **135**, 13326-13329.
31. M. Zhang, G. Feng, Z. Song, Y.-P. Zhou, H.-Y. Chao, D. Yuan, T. T. Y. Tan, Z. Guo, Z. Hu, B. Z. Tang, B. Liu and D. Zhao, *Journal of the American Chemical Society*, 2014, **136**, 7241-7244.
32. B. Icli, E. Solari, B. Kilbas, R. Scopelliti and K. Severin, *Chemistry*, 2012, **18**, 14867-14874.
33. Q. Gong, Z. Hu, B. J. Deibert, T. J. Emge, S. J. Teat, D. Banerjee, B. Mussman, N. D. Rudd and J. Li, *Journal of the American Chemical Society*, 2014, **136**, 16724-16727.
34. S. J. Clark, Segall, M.D., Pickard, C.J., Hasnip, P.J., Probert, M.J., Refson, K. Payne, M.C, *Z Kristallogr* 2005, **220**, 567-570.
35. Jmol: an open-source Java viewer for chemical structures in 3D. , <http://www.jmol.org/>, 2015).
36. R. S. B. Anushri Rananaware, Hemlata Patil, Mohammad Al Kobaisi, Amanda Abrahamama, Ravi Shukla, Sidhanath V. Bhosale, Sheshanath V. Bhosale, *RSC Advances*, 2014, **4**, 59078-59082.
37. <http://webbook.nist.gov/chemistry/fluid/>
38. J. J. L.Czepirski, *Chem. Eng. Sci.*, 1989, **44**.
39. R. W. Seidel and I. M. Oppel, *Structural Chemistry*, 2009, **20**, 121-128.
40. K. Tan, N. Nijem, P. Canepa, Q. Gong, J. Li, T. Thonhauser and Y. J. Chabal, *Chemistry of Materials*, 2012, **24**, 3153-3167.
41. K. Sumida, D. L. Rogow, J. A. Mason, T. M. McDonald, E. D. Bloch, Z. R. Herm, T. H. Bae and J. R. Long, *Chemical reviews*, 2012, **112**, 724-781.